Available online at www.sciencedirect.com
ScienceDirect
Ceramics International 35 (2009) 2203–2212
CERAMICS INTERNATIONAL
www.elsevier.com/locate/ceramint

Degradation of MgO–C refractories by MnO-rich stainless steel slags

Marie-Aline Van Ende *, Muxing Guo, Peter Tom Jones, Bart Blanpain, Patrick Wollants

Department of Metallurgy and Materials Engineering, Katholieke Universiteit Leuven, Kasteelpark Arenberg 44 box 2450, B-3001 Leuven, Belgium

Received 29 September 2008; received in revised form 25 October 2008; accepted 22 December 2008
Available online 22 January 2009

Abstract

In order to identify the influence of MnO on the wear rate of MgO–C bricks for the production of high Mn stainless steel, MgO–C refractory samples were exposed to slags containing different MnO levels (up to 26 wt.%). Although the investigations of the worn brick microstructures revealed the presence of numerous Mn-rich metal particles and the formation of a (Mg,Mn)O solid solution at the slag/refractory interface, no clear evidence of wear rate enhancement was observed due to high MnO concentration in the slags. With respect to refractory wear, the MgO content in the slag is the dominant factor. The degradation processes are discussed by combining experimental results and thermodynamic calculations.

Keywords: C. Corrosion; D. MgO; E. Refractories

1. Introduction

The increase of the Ni price has a heavy impact on the production cost of austenitic stainless steel. Given the current economic situation, the Ni price is expected to remain high, resulting in the development of Ni-free stainless steels [1]. Recent research and publications [2–6] show that, regarding the producibility and the mechanical properties of the final product, the combination of C, N with Cr and Mn can efficiently replace Ni. The required Mn level (12–25 wt.%) is much higher than presently achieved in carbon steelmaking. As a result, limited information is available regarding the metallurgical process. In particular, the behaviour of the refractory materials used in the standard stainless steel production route in contact with Mn-rich melts must be investigated.

The interactions between Ni-free austenitic stainless steel (12 wt.% Mn, 18 wt.% Cr) and slags were experimentally studied by the present authors [7]. It was found that part of the Mn is inevitably oxidized to the slag. High MnO slag levels may enhance the degradation of MgO–C bricks, which are commonly used as refractory material for the electric arc furnace (EAF) linings.

Ikesue et al. [8] showed that the corrosion rate of MgO–C refractory bricks increased with higher MnO_x contents in a basic (C/S = 3) CaO–SiO_2–Al_2O_3–MnO_x–Fe_tO slag with total Mn and total Fe of, respectively, 6.5–16.8 wt.% and 10 wt.%. They reported that the use of MnO_x-rich slag maintained the total Fe content in slag high, as a result of the Mn–Fe exchange reaction between slag and steel. Moreover, this slag showed higher soluble MgO content. The combination of high total Fe content and high MgO saturation solubility in slag might have caused enhancement of refractory wear. Metallic Fe was observed at the slag/refractory interface, resulting from refractory carbon oxidation by FeO_x. With SiO_2–Al_2O_3–CaO–MnO slags containing 6.55–32.9 wt.% MnO, Xie et al. [9] found metallic Mn particles at the refractory/slag interface. Although they noticed a larger chemical attack by the slag richer in MnO, they concluded that the reaction between the refractory carbon and MnO was limited as long as the periclase grains do not suffer from severe slag attack. Differences in thermodynamic driving forces and kinetic restrictions were suggested to explain the lower wear rate observed with MnO, compared to FeO. In both studies, it was reported that the presence of strong reacting compounds towards the periclase grains and the refractory carbon, such as FeO_x and Al_2O_3, led to a weakened brick microstructure. However, such slag systems are substantially different from a stainless steel slag containing lower FeO_x and Al_2O_3 levels.

In the present work, MgO–C refractory samples were immersed in distinct CaO–SiO_2–MgO–Al_2O_3–Cr_2O_3–MnO

* Corresponding author. Tel.: +32 16 321318; fax: +32 16 321991.
E-mail address: MarieAline.VanEnde@mtm.kuleuven.be (M.-A. Van Ende).

0272-8842/$34.00
doi:10.1016/j.ceramint.2008.12.007

slags containing up to 26 wt.% MnO for different time lengths to investigate the influence of MnO on the degradation of MgO–C refractories. The worn microstructures were investigated and the wear rate was assessed by evaluating the changes in sample dimensions and weight. Thermodynamic calculations were performed using FactSage software and were compared with the experimental results.

2. Experimental

2.1. Materials preparation

The composition of the slag samples is listed in Table 1. Initially, industrial slag was crushed and mixed to obtain a homogeneous slag. The necessary amount of Mn oxide powder (reagent grade) was mixed to obtain the MnO-containing slags F2 and F3. Silica was added to the slags F1 and F2 to lower their basicity.

The refractory samples were cut from a commercially available pitch-bonded magnesia-carbon refractory brick (5.5 wt.% residual carbon) in cylinders of about 45–50 mm height and a diameter of approximately 16 mm.

2.2. Experimental set-up and procedure

The experimental apparatus is illustrated in Fig. 1a. 200 g of slag mixture was filled in a Mo crucible (diameter 40 mm, height 85 mm) and heated in a high temperature vertical tube furnace (GERO HTRV 100-250/18, with $MoSi_2$ heating elements) under a protective Ar atmosphere. The refractory samples were fixed on a 3-mm diameter Mo rod (Fig. 1b). When the melt temperature reached 1600 °C, the refractory sample, initially kept near the top of the furnace, was moved down and maintained above the Mo crucible for 10 min to preheat and remove the binder in the brick. Subsequently, the refractory sample was immersed into the molten slag for a determined time. Three refractory samples were consecutively immersed without renewing the slag**.** After these three successive immersions, the remaining slag was cooled down to room temperature. This procedure was then repeated for the two other slag systems (F2 and F3). The experimental conditions are summarised in Table 2.

Table 1
Slag compositions before and after the tests, as determined by XRF analysis (in wt.%).

Slag	CaO	Al_2O_3	SiO_2	MgO	Cr_2O_3	MnO	FeO	Basicity
F1								
Before	43.1	1.0	38.5	10.4	1.4	0.5	1.1	1.39
After	41.4	0.9	35.5	17.5	<0.1	0.4	<0.1	1.66
F2								
Before	36.6	0.7	34.6	8.7	1.2	13.4	1.0	1.31
After	38.2	0.9	32.6	16.3	0.2	6.9	<0.1	1.67
F3								
Before	34.6	3.0	23.0	4.8	2.2	26.1	0.9	1.71
After	38.3	3.3	25.6	8.6	1.2	16.4	<0.1	1.83

The basicity is defined as $(CaO + MgO)/SiO_2$.

2.3. Sample analysis techniques

Before cutting perpendicular to the refractory/slag interface at 10 mm from the bottom, the corroded refractory samples were cold mounted in low viscosity resin (Epofix) by vacuum impregnation to prevent the damaged refractory grains to be removed. The surface situated at 10 mm from the bottom of the sample was polished and coated with a conducting carbon layer for microstructural characterisation. The degradation of the refractory samples was evaluated by the changes in sample dimensions, weight, cross-sectional area, and slag composition.

Compositional analyses were performed with an electron probe microanalysis (EPMA, JEOL JXA-733) coupled with an energy dispersive spectrometer (EDS). The composition was determined using a semi-quantitative routine. Additional images and chemical analyses were obtained with a high-resolution scanning electron microscope (Philips SEM XL-30 FEG), equipped with an EDS detector system from EDAX.

Initial slags and final slags after the tests were analysed with a wavelength-dispersive X-ray fluorescence spectrometer (WDXRF) from Philips (PW2400 sequential X-ray spectrometer). After being crushed, the slags were fused in a homogeneous glass bead using a fully automatic bead preparation system (PANalytical Perl'X 3). Quantitative analyses were performed by using standard reference slags (British Chemical Standards series) to provide a calibration curve.

2.4. Thermodynamic calculations

Thermodynamic calculations were performed using the FactSage software version 5.4.1 [10]. The equilibrium module EQUILIB, which is based on the minimisation of the Gibbs free energy, was used with the FACT databases (FACT-MONOA, FACT-SLAGA and FACT-FeLQ). Argon (10 g) was included in the system to take into account the atmosphere surrounding the samples. The slag-refractory interactions were modelled at 1600 °C by successive additions of MgO–C refractory (parameter α in g) containing 6 wt.% C to 100 g of slag F1, F2 or F3 (Table 1). For example, when α = 10 g, the equilibrium calculations were conducted with 9.4 g MgO, 0.6 g C and 100 g of slag. The ratio of slag amount to that of refractory used in the experiments corresponds to α = 15 g.

3. Results and discussion

3.1. General overview

The weight loss and the measured wear rates of the refractory samples exposed to the slags are shown in Fig. 2. The wear rate was evaluated from the change in average diameter and height (determined by three measurements) of the refractory samples after the tests. No data could be provided for samples F2-2 and F3-2 because the measurement capability of the instruments was not adequate for evaluating small changes in dimension and weight. The samples F1-1, F2-1 and F3-1, which were immersed first in their respective slags,

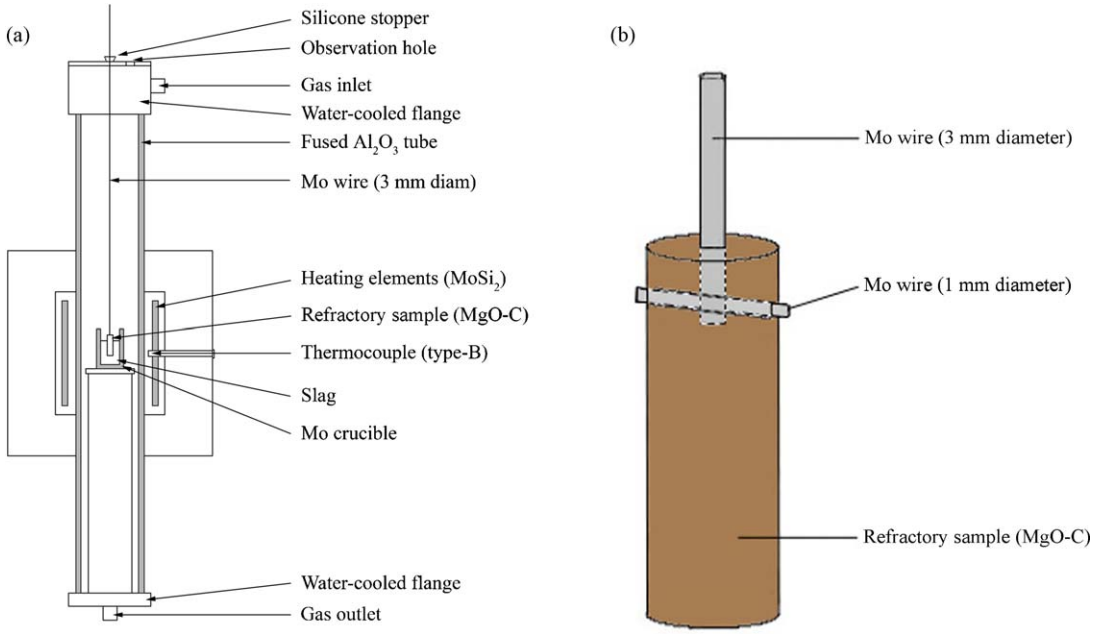

Fig. 1. Schematic drawings of (a) the vertical tube furnace for the tests and (b) the connection between the Mo wire and the refractory sample.

suffered the greatest loss in terms of weight and size in comparison with the following ones. A picture of samples F1-1, F1-2 and F1-3 after corrosion is provided in Fig. 3 and shows that the degradation was very intense for sample F1-1 compared to F1-2 and F1-3. However, as seen in Fig. 2, sample F3-1 immersed in slag with a higher basicity and a higher MnO content is much less damaged with respect to samples F1-1 and F2-1. Macroscopically, the origin of high wear rates seems to be attributed to the low MgO levels in the slag and low basicity. Once MgO saturation was reached, the wear rates decreased drastically.

The corroded microstructures of the refractory sample immersed in slag F1 for different time lengths are shown in Fig. 4. The hot face of the worn refractory brick samples consists of a decarburised, slag infiltrated zone, of approximately 500 μm–1 mm thickness. The overview of the hot face of the refractory samples clearly demonstrates the efficiency of the carbon phase to block the infiltration of the slag in the brick (Fig. 4a). The intergranular slag infiltration was very limited.

Table 2
Experimental conditions.

Refractory sample	Slag	Order of immersion	Immersion time (min)
F1-1	F1–<1 wt.% MnO	1	45
F1-2		2	20
F1-3		3	45
F2-1	F2–13 wt.% MnO	1	45
F2-2		2	20
F2-3		3	45
F3-1	F3–26 wt.% MnO	1	40
F3-2		2	45
F3-3		3	60

However, intragranular slag attack was observed in the sintered grains, leading to the gradual disintegration and the removal of the MgO subgrains to the slag (Fig. 4c) and allowing the slag to infiltrate deeper in the brick. Erosion of the brick was also noticed in samples F1-2 (Fig. 4c) and F1-3 (Fig. 4d). The slag phase, whose average composition is listed in Table 3, was in general heterogeneous due to crystallisation upon cooling. Few metal particles are located at the slag/refractory interface of samples F1-1, F1-2 and F1-3 (Fig. 4a–d).

Fig. 5 shows the worn microstructures of the refractory samples after corrosion by slag F2. The thickness of the decarburised zone was less than 1 mm in all three samples (Fig. 5a–c). Similar as with the refractory samples in contact with slag F1, MgO grains were detached from the brick surface and dispersed in the slag phase. The sintered periclase grains in contact with the slag were infiltrated along the subgrains. In

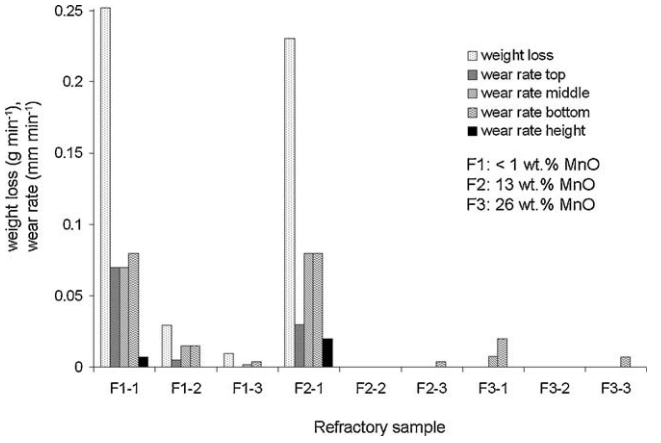

Fig. 2. Weight loss (in g min^{-1}) and wear rates (in mm min^{-1}) of the refractory samples after exposure to slags. Wear rates include the changes in dimension of the cross-section at the top, middle and bottom of the sample and of the height.

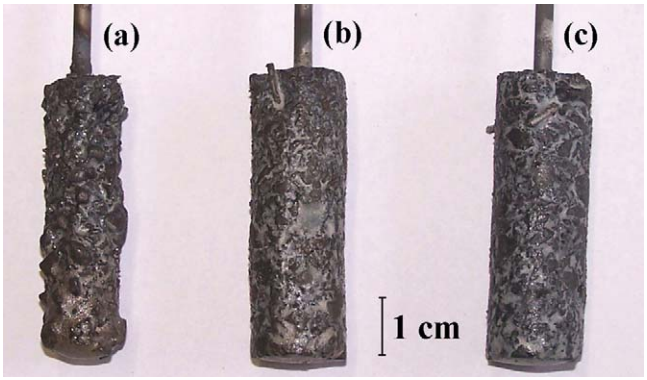

Fig. 3. Digital image of the degraded MgO–C samples consecutively dipped in slag F1: (a) first refractory sample immersed during 45 min (F1-1); (b) second refractory sample immersed during 20 min (F1-2); (c) third and last refractory sample dipped during 45 min (F1-3).

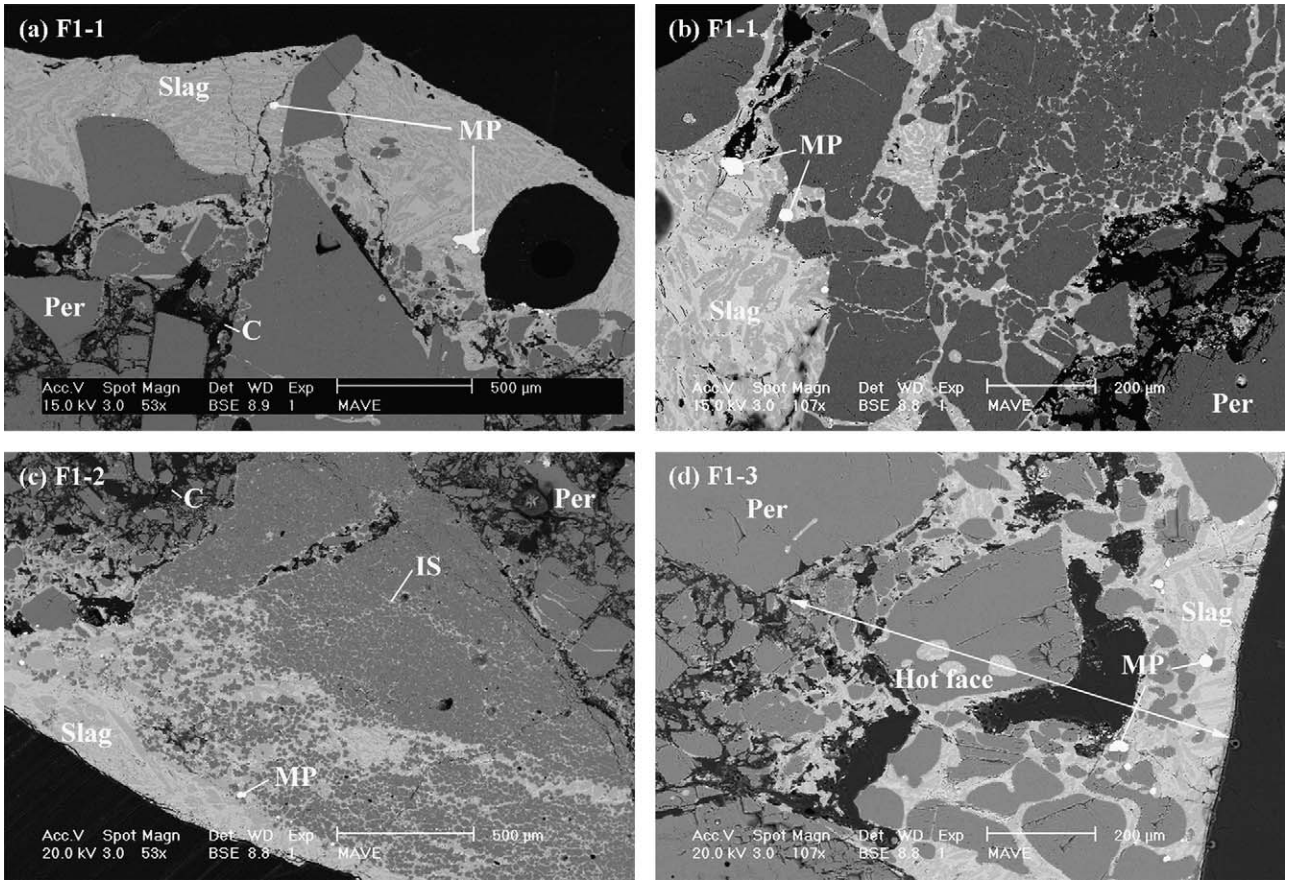

Fig. 4. SEM (backscattered electron) images of the worn refractory samples immersed in slag F1 ($B = 1.39$). (a) Overview of the reaction zone and (b) enlarged view of the hot face of the worn brick after an immersion time of 45 min (F1-1, MgO unsaturated slag); (c) intragranular infiltration of a sintered grain by slag and subsequent removal of the grains in the slag (brick with an immersion time of 20 min—F1-2); (d) hot face of the worn brick after an immersion time of 45 min (F1-3). Per: periclase grain; MP: metal particle; C: carbon phase; IS: infiltrating slag.

Table 3
Average chemical compositions of the infiltrated slag found in the worn brick microstructure, as determined by EPMA analysis (in wt.%).

Slag	CaO	SiO_2	MgO	MnO	Cr_2O_3	Al_2O_3	TiO_2
F1	35–55	35–40	6–25	–	<0.5	<2	–
F2	34–48	35–39	9–20	4–11	<0.5	<1	–
F3	30–50	26–40	10–25	3–11	<0.5	–	0.5–1.5

contrast with previous observations, numerous metal particles were found at the hot face of all three samples.

Compared to the worn microstructures after corrosion by the slags F1 and F2, erosion of the periclase grains was limited with slag F3 (Fig. 6). However, intragranular slag infiltration in sintered periclase grain took place, resulting in a slag penetration depth of about 1 mm. Small MgO grains and the edges of large ones directly adjacent to the slag are brighter than the unreacted periclase. This suggests that they are chemically

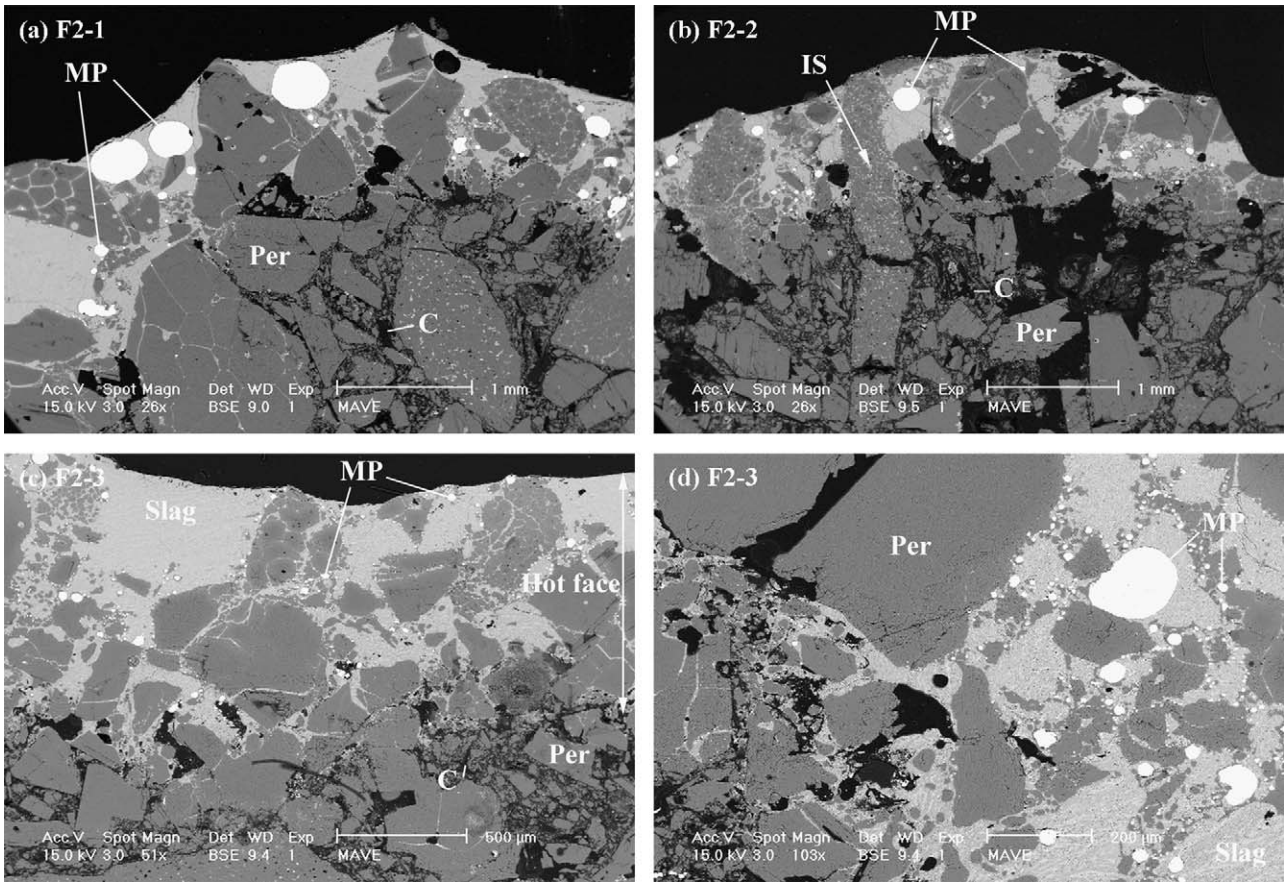

Fig. 5. SEM (backscattered electron) images of the three worn bricks immersed in slag F2: Overview of the hot face zone after an immersion time of (a) 45 min (F2-1, MgO unsaturated slag) and (b) 20 min (F2-2); (c) Hot face area and (d) enlarged view of the decarburised zone/refractory interface of refractory sample immersed 45 min (F2-3). Presence of numerous metal particles. Per: periclase grain; MP: metal particle; C: carbon phase; IS: infiltrating slag.

altered by a high atomic number element provided by the slag. Numerous metal particles were also found at the slag/refractory interface in all three samples.

The main corrosion mechanisms observed in worn refractory samples consist of slag infiltration, erosion and dissolution of the periclase grains and oxidation of the refractory carbon by reducible slag components. MgO dissolution appears to be the most critical mechanism, causing severe wear of the refractory when the infiltrating slag is not saturated with MgO. Adding MnO to the slag did not cause any appreciable enhancement in corrosion rate.

3.2. Direct and indirect carbon oxidation

Fig. 7a shows the evolution with parameter α at the temperature of 1600 °C of the main species in the gas and carbon phases of slag F1. Carbon as a solid phase appears in the system when α reaches 18.9 g. The gaseous products include CO(g), Mg(g), Mn(g), SiO(g), and CO_2(g). With increasing MnO content in slag F2 (Fig. 7b), the solid carbon phase does not appear in the given range of α. The gaseous products are the same as those described in Fig. 7a, except that the amount of Mn(g) is larger.

The decarburisation of the refractory hot zone is mainly caused by the direct carbon burnout by gaseous oxygen (reaction (1)) and by the MgO–C reaction [11–18] (reaction (2)):

$$C(s) + \tfrac{1}{2}O_2(g) = CO(g) \quad (1)$$

$$MgO(s) + C(s) = Mg(g) + CO(g) \quad (2)$$

Reaction (2) is also referred to as the intrinsic carbon oxidation [19]. The presence of Mg(g) in the gas phase in the thermodynamic predictions indicates the occurrence of the MgO–C reaction. Low oxygen partial pressures (10^{-11} to 10^{-14} atm) and high temperatures generate favourable conditions for the MgO–C reaction to occur, resulting in large decarburised zones strongly attacked by the slag in the brick microstructure, as observed in the extended slag line zone in vacuum oxygen decarburisation (VOD) ladles [19]. In the present observations, the decarburised and slag infiltrated zones in the worn refractory samples were very limited, indicating that the MgO–C reaction did not significantly take place as compared with the situation in the VOD-ladle. The higher oxygen partial pressure during the present tests (10^{-5} to 10^{-6} atm) in combination with the slow removal of the gaseous reaction products and the CO(g) build-up at the interface through the hot face may slow down or even prevent this reaction to occur.

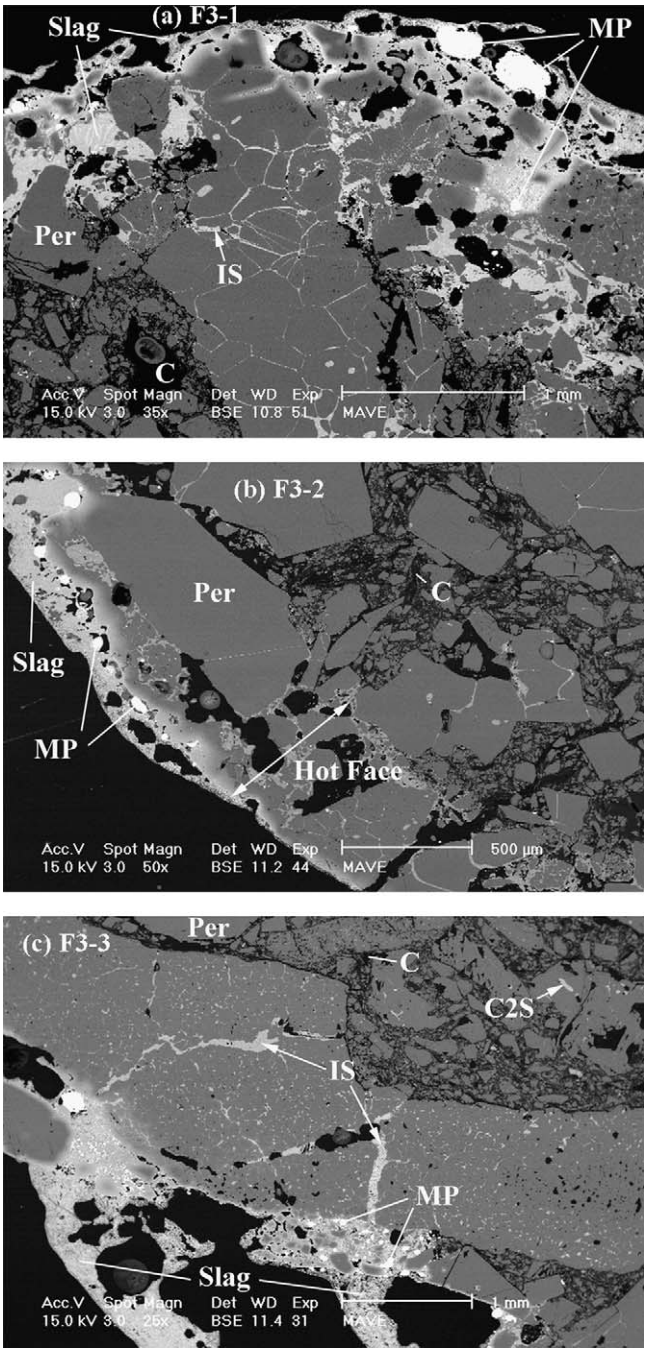

Fig. 6. SEM (backscattered electron) images of the three worn samples immersed in slag F3. (a) Overview of the hot face zone after an immersion time of 40 min (F3-1, MgO unsaturated slag). Presence of large metal particles and infiltrating slag along the grain boundaries of sintered grains; (b) view of the sample hot face and occurrence of metal particles at the slag/refractory interface after an immersion time of 45 min (F3-2); (c) view of slag infiltration along grain boundaries in large sintered periclase grain forming sample F3-3 (immersion time of 60 min). Numerous metal particles in the infiltrating slag, at the refractory/slag interface. Per: periclase grain; MP: metal particle; C: carbon phase; IS: infiltrating slag.

3.3. MgO dissolution and detachment

The slag compositions before and after the consecutive immersion of three MgO–C refractory samples are shown in Table 1. A substantial increase of the MgO content was measured, as depicted in Fig. 8a. The increase of the MgO slag content is more considerable in slags F1 and F2 than in F3. It is reasonable to think that the principal source of MgO in the slags comes from the first sample, which underwent the most significant material loss and the highest wear rate (Fig. 2). According to the mass balance for MgO (based on slag weight and composition), the amount of MgO in the slag increased with approximately 15 g during the tests with slags F1 and F2, and about 8 g for slag F3. These values are in agreement with the total weight loss of the refractory samples dipped successively in the same slag.

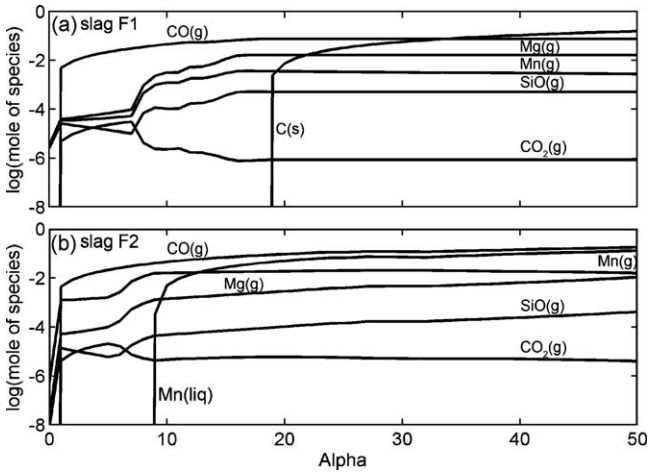

Fig. 7. Prediction of the main species in gas, liquid metal and solid phases for 100 g of (a) slag F1 (low basicity and low MnO) and (b) slag F2 (low basicity and medium MnO) with increasing amount of MgO–C refractory (α in g) at 1600 °C.

The other major change in the slag compositions after the test concerns the Cr_2O_3 and MnO contents. Table 1 reveals that slags F1, F2 and F3 are seriously depleted in Cr_2O_3 after the tests. As seen in Fig. 8b, the MnO content in slags F2 and F3 was significantly decreased after the immersion tests.

Fig. 9a and b depict the evolution, according to FactSage calculations, of respectively the MgO and MnO contents in the slag phase with parameter α for slags F1, F2 and F3. The

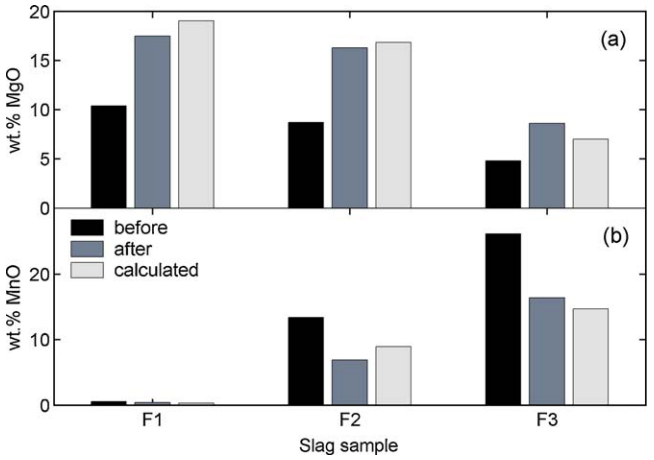

Fig. 8. (a) MgO and (b) MnO slag contents (wt.%) measured before and after the tests compared to the calculated values for α = 15 g.

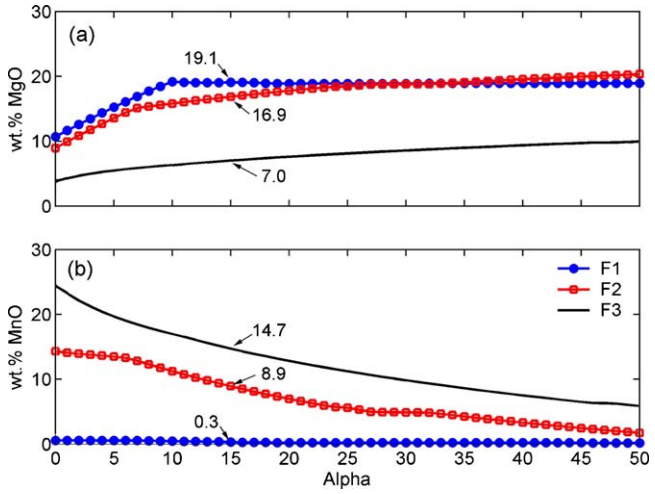

Fig. 9. Prediction of the evolution of (a) the MgO content (wt.%) and (b) the MnO content (wt.%) in the slag phase with increasing amount of MgO–C refractory (α in g) at 1600 °C for slags F1, F2 and F3.

evolution of the (Mg,Mn)O solid solution weight is illustrated in Fig. 10a, while its composition is given in Fig. 10b in terms of the MgO content, with the remainder being MnO. In the case of slag F1, with increasing α, the MgO content in the slag increases until the MgO solid phase appears at $\alpha = 10$ g and then remains constant. The MnO content in the MgO solid phase is less than 1 wt.% (Fig. 10b).

Recalculation for slag F2 shows that the solid solution appears at a lower α value (7 g) and contains a lower MgO level than for slag F1. At this value, the MnO content in the solid solution reaches a maximum of 28.5 wt.% and decreases with increasing α. In the liquid slag, the MgO content increases from 9 to 20 wt.% with increasing α, while the MnO level decreases from 14.3 to 2.3 wt.%. At the start the decrease is gentle and then it becomes more considerable when the solid solution appears in the system at $\alpha = 7$ g.

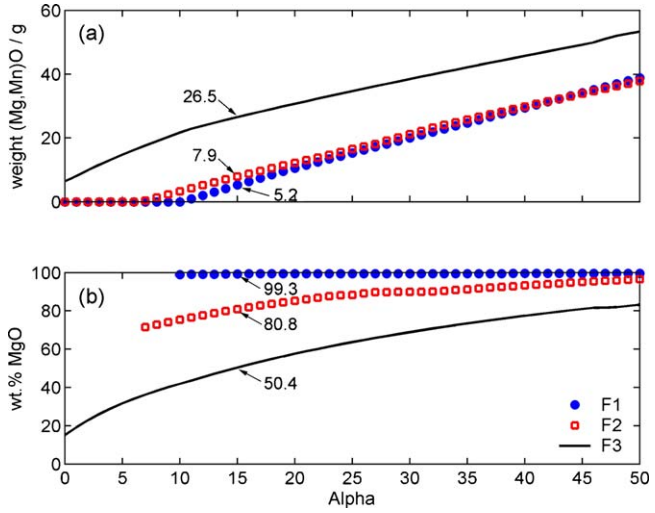

Fig. 10. Evolution of (a) the amount of (Mg,Mn)O solid solution and (b) the MgO content (wt.%) in the (Mg,Mn)O solid solution with increasing amount of MgO–C refractory (α in g) at 1600 °C for slags F1, F2 and F3, as predicted by FactSage.

The influence of a higher MnO content and a higher basicity is examined with slag F3. As seen in Fig. 10a, the solid solution exists even if no refractory is included in the system ($\alpha = 0$), indicating that the slag is oversaturated with respect to MnO and MgO. For this α value, the solid solution weights 6.5 g and contains about 19.5 wt.% MgO and 80.5 wt.% MnO. The MgO content in the solid solution increases with α. In the slag phase (Fig. 9a), the MgO content is lower than in the slags F1 and F2 and increases slightly with α.

The calculated MgO saturation levels in slags F1, F2 and F3, for $\alpha = 15$ g, are, respectively, of 19.1 wt.%, 16.9 wt.% and 7.0 wt.% (Fig. 9a). These values are compared with the experimental results in Fig. 8a. As can be seen, the predictions are in good agreement with the experimental results. Moreover, it reveals that the difference between initial and equilibrium MgO contents, defining the driving force for MgO dissolution, was substantially larger with slags F1 and F2 compared to F3.

The thermodynamic predictions indicate that slags F1 and F2 at the initial conditions are not saturated in MgO since a solid MgO phase only appears when $\alpha > 0$. The severe degradation of the refractory samples immersed at first in the slags corroborates these predictions. For these samples (F1-1 and F2-1), the driving force for MgO dissolution was significant (Fig. 8a), leading to a fast dissolution of the MgO grains in the liquid slag. The large driving force can be explained by the MgO solubility, which is influenced by basicity. Indeed, the MgO saturation level decreases with basicity [20], which is also predicted by the calculations. The slags F1 and F2, characterised by a low initial basicity, have a higher MgO solubility than in slag F3, therefore increasing the driving force for MgO dissolution. On the other hand, the more basic slag F3 led to a less degraded microstructure. Lower wear rates were observed, because the MgO solubility and, subsequently, the driving force was lower. MgO saturation is thus an essential component of sound slag engineering. Compared to the MnO slag level, the choice of an appropriate MgO slag content is more critical regarding refractory degradation.

3.4. Reaction between refractory carbon and reducible slag components

Numerous metal particles, containing Mn, Cr, and Fe, were found within the hot face of the worn brick, especially in the samples corroded by MnO-rich slags. Their compositions (Table 4) vary both between and within samples. The Mn content in the metal particles is in general lower in the samples dipped first in the slag (F3-1, F1-1 and F2-1) and rises with the MnO slag content. However, the highest Mn content in the metal particles was found in the refractory samples F2-2 and F2-3, instead of the samples in contact with slag F3 containing 26 wt.% MnO. In the low MnO containing slags, Cr is the dominant element, followed by Fe.

These metallic particles result from the oxidation of the refractory carbon by the reducible components from the slag, such as FeO_x, CrO_x, MnO, SiO_2, referring to extrinsic carbon oxidation [18,19]. The consumption of the reducible components with the refractory carbon is also corroborated by the

Table 4
Average chemical composition of the metal particles found at the refractory/slag interface on the worn brick microstructure, as determined by EPMA analysis (in wt.%).

Slag	Refractory sample	Cr	Fe	Mn
F1	F1-1	65–90	10–30	0–10
	F1-2	50–90	10–40	2–10
	F1-3	70–80	10–20	5–10
F2	F2-1	45–60	10–30	20–30
	F2-2	10–50	<10	40–90
	F2-3	30–55	<10	40–70
F3	F3-1 to 3	50–65	25–30	5–20

strong decrease in the CrO_x and MnO contents measured in the infiltrating slag in the refractory hot zone (Table 3) as well as in the final slag after the tests (Table 1).

The evolution of the predicted species in the liquid metal phase with parameter α for slags F2 and F3 is shown in Fig. 11. Extrinsic carbon oxidation reactions take place, resulting in the formation of a liquid metal phase when $\alpha > 0$ and in the decrease of the MnO slag content with α (Fig. 9b). For both slags, liquid Fe forms first, followed by the formation of a liquid Fe–Cr phase through the reduction of FeO and Cr_2O_3. The reduction of MnO becomes significant when most of the FeO and Cr_2O_3 is reduced. The formation of liquid Mn with slag F3 is, therefore, shifted to higher α values owing to a higher Cr_2O_3 slag content compared to slag F2. The calculation results in Fig. 10 were experimentally verified by the formation of numerous metal particles at the slag/refractory interface of the samples immersed in the MnO-rich slags F2 and F3, compared to F1 (Figs. 4–6). The higher Fe and Cr contents measured in the metal particles of the samples immersed first in the slag (Table 4) are consistent with the predicted order of reduction. The Mn content in the metal particles observed in samples F3-1 to F3-3 remains low compared to samples F2-2 and F2-3, though the MnO slag content had doubled. This is in agreement

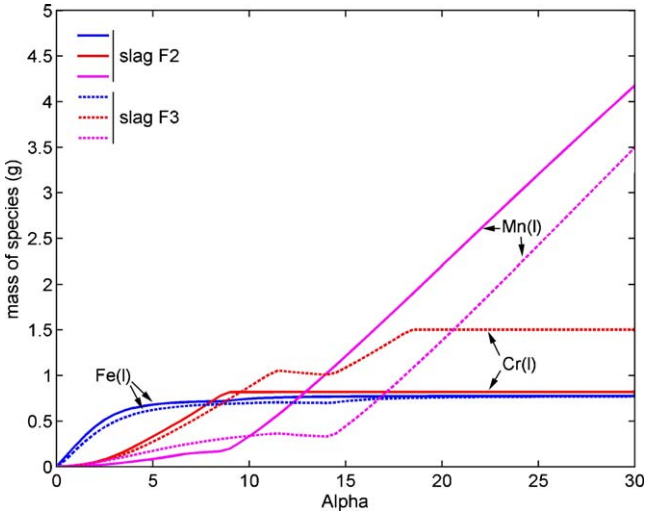

Fig. 11. Prediction of the main species in the liquid metal phase for 100 g of slags F2 (solid lines) and F3 (dashed lines) with increasing amount of MgO–C refractory (α in g) at 1600 °C.

with the calculations, which showed that a higher Cr_2O_3 content retards the MnO reduction. In addition, the experimental observations revealed that the dissolution of MnO in the periclase grains (see Section 3.5) was considerable in samples F3-1 to F3-3, causing a severe depletion in MnO of the infiltrating slag (Table 3). Less MnO can, therefore, be transferred to the reaction sites (slag/carbon interface).

According to the thermodynamic calculations, an increasing MnO content would enhance the oxidation of the refractory carbon. Experimentally, the influence of the MnO level in the slag on the wear rate was found to be very limited (Fig. 2). The poor wetting behaviour of the refractory carbon phase towards the slag limits the contact area between the slag and the refractory, preventing carbon oxidation. Because intrinsic carbon oxidation did not significantly take place, the decarburised area is limited in volume, thereby restricting further slag penetration and reaction between the reducible components of the slag and the refractory carbon.

The latter substantiated that the most harmful contribution to refractory wear comes from the use of MgO unsaturated slag, enabling rapid and severe MgO dissolution in the infiltrating slag.

3.5. Formation of (Mg,Mn)O solid solution

While no Mn was detected in the periclase grains in the three worn refractory samples in contact with slag F1, the formation of a (Mg,Mn)O solid solution was observed in the refractory samples in contact with the MnO-rich slags. The Mn level in the solid solution depends on that of the surrounding slag. Concerning the tests with slag F2, less than 2 wt.% MnO was detected in the MgO particles at the hot face of the first sample (F2-1). Whereas in the two following samples (F2-2 and F2-3), the small MgO particles in the decarburised zone contain up to 16 wt.% MnO. Larger MgO grains contain less than 1 wt.% MnO. This implies that the MnO dissolution in MgO and the formation of the solid solution rarely occur with MgO unsaturated slag, because MgO dissolution in the slag probably proceeds faster than MnO dissolution in MgO. Up to 35–40 wt.% MnO and 4 wt.% Cr_2O_3 were measured in the MgO grains at the hot face of the samples resulting from the tests with slag F3. In the vicinity of the original brick structure, the MnO content of the solid solution falls to less than 10 wt.% MnO.

According to the thermodynamic equilibrium calculations performed with slags F2 and F3 (Fig. 10b), the formation of a (Mg,Mn)O solid solution takes place. The phase diagram of the system MgO–MnO [21] indicates complete miscibility between MnO and MgO at 1600 °C. The MnO content in the solid solution decreases with the refractory amount (α) and is significantly higher with slag F3. For instance, the solid solution contains, for α = 15 g, 19.1 wt.% and 48.9 wt.% MnO for, respectively, slags F2 and F3. As predicted and observed experimentally, the conditions in slag F3 compared to those in slag F2 promoted the MnO dissolution in the periclase grains. After the tests, the MnO loss from the slags F2 and F3 amounts, respectively, to about 10 g and 15 g. From a mass balance estimation, 80–90% of the MnO loss from slag F3 was due to

dissolution in the periclase, the remainder taking part principally in refractory carbon oxidation. In the case of slag F2, only 50–60% of the MnO loss was due to dissolution in MgO.

The formation of a (Mg,Mn)O solid solution occurs by diffusion and exchange of cations between the periclase grain and the slag phase surrounding the former, so as to maintain the electroneutrality of the solid solution particles (reaction (3)) [22–25].

$$Mn^{2+}{}_{(slag)} + Mg^{2+}{}_{(periclase)} = Mn^{2+}{}_{(periclase)} + Mg^{2+}{}_{(slag)} \quad (3)$$

According to this exchange mechanism, the dissolution of MnO in periclase induces the release of MgO in the slag at the refractory hot zone. This was substantiated by comparing the compositions of the initial and the final slag after the tests (Table 1) and those of the infiltrating slag (Table 3). In the case of slag F3, the infiltrating slag composition in terms of MnO and MgO contents differs significantly from the initial and the final slag after the test, testifying that the solid solution formation is more pronounced compared to slag F2. As a result of the exchange reaction, the infiltrating slag is severely depleted in MnO and enriched in MgO.

The presence of a solid solution instead of pure MgO brings the MgO activity in the solid phase below unity. As a result, the MgO solubility in the slag does not reach its maximum value, but varies according to the MnO level. Therefore, even after immersion of several refractory samples, the Mn^{2+}–Mg^{2+} exchange mechanism between the slag and the periclase grains is still possible.

Zhang et al. [26] also found Fe and Mn oxides in the MgO grains at the MgO/slag interface after 3 and 6 h corrosion by a model EAF slag containing 17.5 wt.% Fe_2O_3 and 8.9 wt.% MnO. They reported that the formation of the (Mg,Fe,Mn)O solid solution at high temperature influenced the slag penetration mechanism. This solid solution phase formed a dense layer at the interface due to the increase in crystal size, partly inhibiting slag penetration. In the present condition, the crystals directly adjacent to the slag do not show significant changes in size, although the measured MnO content is high. The immersion time, limited to maximum 45 min, was presumably not long enough to observe growth of the solid solution crystals (MgO grains must be almost saturated with respect to MnO before growth of the solid solution occurs). Further investigations are necessary to confirm this.

From a thermodynamic point of view, there are no restrictions for the reverse reaction (3) to occur if the MgO–MnO solid solution is in contact with a slag containing minor or near zero levels of MnO. In that case, Mn^{2+} would return to the slag phase.

3.6. Industrial relevance

The potential degradation enhancement caused by MnO-rich slags was highlighted by the thermodynamic calculations. However, the choice of a relevant α value to provide a good comparison with the experimental results is not straightforward. The calculation assumes that all compounds and phases are in perfect contact with each other, which is not the case in reality. The poor wetting behaviour of the carbon towards the slag is one of the limiting factors. Moreover, kinetic limitations due to chemical reactions and/or diffusion processes are not considered in the thermodynamic calculations. Despite these limitations, thermodynamic calculations associated with experimental observations can be used to understand the possible reactions between the slag and the magnesia-carbon brick.

The experimental observations and the thermodynamic calculations have indicated that MnO reacts with MgO grains and carbon, which may alter the performance of MgO–C bricks. The loss of MnO in the slag phase ranged between 8 and 10 wt.% after less than 1 h in contact with MgO–C refractory samples. The reason is the considerable amount of refractory with respect to the amount of slag used in the present experimental configuration, amplifying all the reactions taking place between the slag and the refractory phase. Even though they will also take place at the slag-lining interface, their relative importance and their consequences are expected to be less outspoken in industrial practice, owing to the lower ratio between the refractory lining surface versus slag amount. In a 110-ton capacity EAF with a 0.25-m slag line height and a 2-mm slag penetration depth in MgO–C refractory lining, the MnO take up by MgO would amount to 17 kg, assuming that all MgO grains occupying the slag infiltrated refractory volume form a (Mg,Mn)O solid solution containing 45 wt.% MnO. The alteration in slag composition provoked by the subsequent, complete dissolution of the (Mg,Mn)O solid solution in 10 tons of EAF slag is, thereby, insignificant.

Despite the fact that some MnO would temporarily be in a solid state, the formation of the solid solution does not seem to cause important threats concerning the mechanical properties of the refractory bricks. MnO possesses the same rock-salt crystal structure and has approximately the same unit-cell dimensions as MgO [22]. Therefore, no volume expansion due to the (Mg,Mn)O solid solution formation was observed nor expected in the microstructure.

Limitations associated with static tests comprise the rapid saturation of the slag with the reaction products, the lack of slag motion and the absence of a temperature gradient in the refractory [18]. Before performing industrial trials, dynamic corrosion tests, which allow slag motion and renewal, would be worthwhile as they could provide additional information to evaluate the corrosion resistance of MgO–C refractories in contact with MnO-rich slags.

4. Conclusions

MgO–C refractory samples were brought in contact with three slags exhibiting different MnO contents, i.e. <1, 13 and 26 wt.%. Based on the macroscopic and microscopic investigations, the following conclusions are derived:

1. Slag penetration in the brick is limited by the refractory carbon phase due to it is non-wetting character. The overall

infiltration is, therefore, limited. Nevertheless, sintered periclase grains are infiltrated intragranularly by the slag, leading to the disintegration and the removal of MgO subgrains in the slag. This problem can be tackled by opting for fused magnesia grains.

2. When immersed in slags unsaturated with MgO, a severe wear rate of the refractory material was observed. In order to limit the degradation of the MgO-based refractories, the use of MgO slag saturation is essential. MgO dissolution was examined with thermodynamic calculations. The results of the predictions are in good agreement with the experimental observations.
3. Metal particles were found at the interface between the slag and the refractory, resulting from extrinsic carbon oxidation. Cr is the major element found in the metal particles for the slag devoid of MnO, while Mn and Cr are both detected in high concentrations for the MnO rich slags. These observations are consistent with thermodynamic calculations. Although the latter showed an increase in carbon oxidation with MnO content, this reaction was limited owing to the non-wettability of carbon by slag and MnO take up by MgO.
4. The formation of a (Mg,Mn)O solid solution was predicted by the thermodynamic calculations and experimentally observed at the hot face of the samples immersed in MnO-rich slags. Although this represents a source of MnO loss, the consequences of the latter on the refractory material are limited from a refractory wear point of view.

Based on these conclusions, and considering that only static corrosion tests were conducted, MnO-rich slags resulting from the production of Ni-free austenitic stainless steel are not expected to cause severe wear of the refractory linings of an EAF unit.

Acknowledgment

The research was funded by a IWT project (project no. 040423) from the Flemish government of Belgium in collaboration with ArcelorMittal Research Industry Gent (OCAS).

References

[1] T. Oshima, Y. Habara, K. Kuroda, Efforts to save nickel in austenitic stainless steels, ISIJ Int. 47 (3) (2007) 359–364.
[2] J. Menzel, W. Kirschner, G. Stein, High nitrogen containing Ni-free austenitic steels for medical applications, ISIJ Int. 36 (7) (1996) 893–900.
[3] P.J. Uggowitzer, R. Magdowski, M.O. Speidel, Nickel free high nitrogen austenitic steels, ISIJ Int. 36 (7) (1996) 901–908.
[4] A. Di Schino, J.M. Kenny, M.G. Mecozzi, M. Barteri, Development of high nitrogen, low nickel, 18%Cr austenitic stainless steels, J. Mater. Sci. 35 (19) (2000) 4803–4808.
[5] G. Stein, J. Lueg, High nitrogen steels—applications in present and future, in: Proceedings of the 3rd International Conference on High Nitrogen Steels, 1993, pp. 31–42.
[6] P.J. Uggowitzer, M. Harzenmoser, Strengthening of austenitic stainless steels by nitrogen, in: Proceedings of the 1st International Conference on High Nitrogen Steels, 1988, pp. 174–179.
[7] M.A. Van Ende, M.X. Guo, P.T. Jones, B. Blanpain, P. Wollants, Manganese and chromium distribution between $CaO–SiO_2–MgO_{sat.}–CrO_{1.5}–MnO$ slags and Fe–Cr–Mn stainless steel, ISIJ Int. 48 (10) (2008) 1331–1338.
[8] A. Ikesue, H. Yamamoto, H. Shikano, K. Hiragushi, S. Kataoka, Corrosion mechanism of MgO–C refractories by manganese oxide containing slag, Taikabutsu (Refractories) 40 (9) (1988) 535–542.
[9] D.S. Xie, C. Garlick, T. Tran, The wear of tundish stopper refractories by inclusion slags, ISIJ Int. 45 (2) (2005) 175–182.
[10] C. Bale, P. Chartrand, S.A. Degterov, G. Eriksson, K. Hack, R. Ben Mahfoud, J. Melancon, A.D. Pelton, S. Petersen, FactSage thermochemical software and databases, Calphad 26 (2) (2002) 189–228.
[11] G.D. Pickering, J.D. Batchelor, Carbon-MgO reactions in BOF refractories, Am. Ceram. Soc. Bull. 50 (7) (1971) 611–614.
[12] R.J. Leonard, R.H. Herron, Significance of oxidation–reduction reactions within BOF refractories, J. Am. Ceram. Soc. 55 (1) (1972) 1–6.
[13] S.C. Carniglia, Limitations on internal oxidation–reduction reactions in BOF refractories, Am. Ceram. Soc. Bull. 52 (2) (1973) 160–165.
[14] J. Pierard, D. Sichen, P. Jonsson, S. Seetharaman, T. Landin, Effect of slag on carbon bearing MgO refractories, Ironmak. Steelmak. 25 (5) (1998) 374–381.
[15] W.E. Lee, R.E. Moore, Evolution of in situ refractories in the 20th century, J. Am. Ceram. Soc. 81 (6) (1998) 1385–1410.
[16] C. Baudin, C. Alvarez, R.E. Moore, Influence of chemical reactions in magnesia-graphite refractories: I. Effects on texture and high-temperature mechanical properties, J. Am. Ceram. Soc. 82 (12) (1999) 3529–3538.
[17] C. Baudin, C. Alvarez, R.E. Moore, Influence of chemical reactions in magnesia-graphite refractories: II. Effects of aluminum and graphite contents in generic products, J. Am. Ceram. Soc. 82 (12) (1999) 3539–3548.
[18] W.E. Lee, S. Zhang, Melt corrosion of oxide and oxide-carbon refractories, Int. Mater. Rev. 44 (3) (1999) 77–104.
[19] S. Smets, S. Parada, J. Weytjens, G. Heylen, P.T. Jones, M. Guo, B. Blanpain, P. Wollants, Behaviour of magnesia-carbon refractories in vacuum-oxygen decarburisation ladle linings, Ironmak. Steelmak. 30 (4) (2003) 293–300.
[20] Slag Atlas, Verlag Stahleisen Gmbh, Düsseldorf, 1995.
[21] Schenk, Slag Atlas, Verlag Stahleisen Gmbh, Düsseldorf, 1995.
[22] T.S. Liu, R.J. Stokes, C.H. Li, Fabrication and plastic behavior of single-crystal MgO–NiO and MgO–MnO solid-solution alloys, J. Am. Ceram. Soc. 47 (6) (1964) 276–279.
[23] S. Mackwell, M. Bystricky, C. Sproni, Fe–Mg interdiffusion in (Mg,Fe)O, Phys. Chem. Miner. 32 (5–6) (2005) 418–425.
[24] J.T. Jones, I.B. Cutler, Interdiffusion in the system $Mn_xO–MgO$, J. Am. Ceram. Soc. 54 (7) (1971) 335–338.
[25] P. Kofstad, Nonstoichiometry, Diffusion, and Electrical Conductivity in Binary Metal Oxides, John Wiley, New York, 1972.
[26] S. Zhang, H. Sarpoolaky, N.J. Marriott, W.E. Lee, Penetration and corrosion of magnesia grain by silicate slags, Br. Ceram. Trans. 99 (6) (2000) 248–255.